# Supplementary Information

## A Physicochemically Compatible Ferrofluid Droplet Robotic System for Automated Bioanalytical Assays

*Christina C. K. Au Yeung[a,b], Ruotong Zhang[a,b], Chengzhi Zhang[a,c], Xiaoxue Fan[a], Yang Cao[a,b], Chi Song[a,b], Haisong Lin[d,e]* and Ho Cheung Shum[b,f]**

[a]Department of Mechanical Engineering, The University of Hong Kong, Hong Kong SAR, China

[b]Advanced Biomedical Instrumentation Centre, Hong Kong Science Park, Shatin, New Territories, Hong Kong SAR, China

[c]Department of Materials Science and Engineering, Southern University of Science and Technology, Shenzhen, Guangdong Province, China

[d]School of Engineering, Westlake University, Hangzhou, Zhejiang Province, China

[e]Research Center for Industries of the Future, Westlake University, Hangzhou, Zhejiang Province, China

[f]Department of Biomedical Engineering and Department of Chemistry, City University of Hong Kong, Hong Kong SAR, China

*Corresponding authors. Email: linhaisong@westlake.edu.cn (Haisong Lin); ashum@cityu.edu.hk (Ho Cheung Shum)

**Note S1 Mediating the optical interference of ferrofluid for sensitive detection in bioanalytical assays**

The integral prerequisite for robust magnetic droplet robotics is the incorporation of sufficient magnetic material responsive to the localized magnetic fields generated for actuation. However, this poses a challenge for applying ferrofluid-based magnetic droplet robots for bioanalytical applications. For these applications, optical detection methods including absorbance, chemiluminescence, and fluorescence, are primarily employed for quantification in analytical reactions and assays. The introduction of additional, often solid or color-bearing, magnetic components will lead to an altered optical profile of the analyte from increased light absorbance and scattering[1,2]. Therefore, it is important to assess the effect of the physical optical properties of the IONPs with different optical detection methods.

IONPs, as evident from their observable color, absorb in the visible light spectrum, and hence is expected to have an impact on absorbance signals. As shown in Fig. S10a, for a substance with an absorbance peak at 530 nm, increasing the concentration of IONP leads to raised background signals and higher absorbance at all wavelengths. As a result, the absorbance signal can no longer be directly correlated with analyte concentration. As IONP concentration increases, the absorbance signal peak eventually becomes drowned out and quantification is no longer possible. To mediate this effect, a suitable optical detection system which minimizes the effect of IONPs on optical signal quantification must be identified. As absorbance is a measure of the ratio of light transmitted ($I$) through a material, it is highly dependent on the incident light ($I_0$). In contrast, direct measurements of light emission ($I_{em}$) signals generated from the reaction itself, such as chemiluminescence, do not have this dependency. Therefore, chemiluminescence-based

detection is expected to be relatively less affected by the addition of light-absorbing material acting to lower the intensity of transmitted light, providing greater signal sensitivity for improved compatibility on the ferrofluid-based droplet robotic system.

To study the effect of IONP on absorbance (ABS) and chemiluminescence (CL) signals, an extensively used quantification technique involving the catalytic reaction of horseradish peroxidase (HRP) with its substrates was studied. The signals were generated from the reaction of HRP with its substrates, 3,3',5,5'-tetramethylbenzidine (TMB) for absorbance and luminol for chemiluminescence, and measured at 650 nm and 425 nm, respectively. Considering IONPs also exhibit peroxidase-like catalytic activity similar to HRP and react with TMB and luminol, IONPs could not be used directly. Instead, colored solutions matching IONP absorbance at each concentration were used to model the effect of adding IONP on optical signal quantification (Fig. S11). The absorbance and chemiluminescence signals, where both HRP and its substrate were present, were measured at each IONP concentration, and compared with the background, where HRP was absent. As expected, as IONP concentration increases, absorbance-based background signals increase rapidly, such that the signal becomes almost overlapped with the background (Fig. S10b, Fig. S12). However, there was relatively little change in chemiluminescence-based signal and background (Fig. S10c, Fig. S12) and a large difference between the signal and background was maintained. To quantitatively compare the results from absorbance- and chemiluminescence-based detection methods, the signal to noise ratios (SNR) were calculated at each IONP concentration (Fig. S10d). The much higher SNR for chemiluminescence-based detection compared to absorbance-based detection, and the relatively low effect of IONP concentration on the SNR confirms that chemiluminescence is a compatible optical detection

method for use in the ferrofluid-based droplet robotic system. The effect of IONP on fluorescence-based detection was also characterized (Fig. S13). Similar to chemiluminescence-based detection, IONP concentration also has little impact on fluorescence signals. However, as an excitation light is required for fluorescence detection, the background signals for fluorescence are generally higher compared to chemiluminescence detection, which is performed in the dark[3], and the resulting SNR remains lower than that for chemiluminescence (Fig. S10d, Fig. S13). Chemiluminescence-based detection remains the optimal detection mechanism to ensure signal sensitivity for optical analysis in ferrofluid-based droplet robotic systems.

In addition, the physical compatibility of different optical detection methods with the integrated droplet robotic device was considered. As a direct consequence of the low path lengths in miniaturized devices, detection based on light absorbance suffers from low sensitivity, as dictated by the Beer-Lambert law[4]. On the other hand, the low path lengths in miniaturized devices could facilitate detection based on light emission, such as chemiluminescence[3,5], by ensuring minimal signal loss from solution absorbance. Similar to the previously described approach, the reaction of HRP with TMB and luminol were used to characterize the effect of IONP light absorbance on optical signal quantification. To study the effect of optical path length, signals from the reaction mixture were measured in standard 96-well plates (path length: 11.5 mm) and the microfluidic chip used in the ferrofluid droplet robotic device (path length: 1.5 mm). By comparing the results obtained with different solution path lengths (Fig. S14), the percentage change in absorbance signals was significantly higher than chemiluminescence signals, decreasing approximately 10-fold, in accordance with the Beer-Lambert Law. Therefore, from

the perspective of both fluid and physical hardware components, chemiluminescence is well-suited for signal detection in the integrated ferrofluid droplet robotic device.

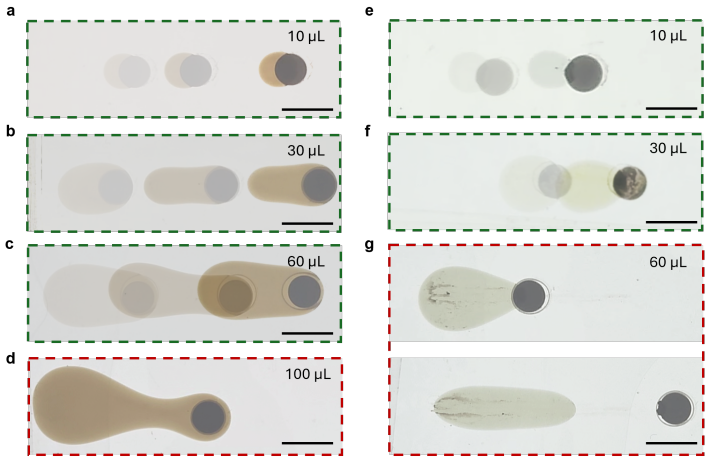


**Fig. S1** (a-c) Actuatable droplet volume of up to 60 µL for colloidal IONP before (d) pinch-off at 100 µL. (e-f) Actuatable droplet volume of up to 30 µL for aggregated IONP before (g) IONP detachment from 60 µL droplet. Scale bars: 5 mm.

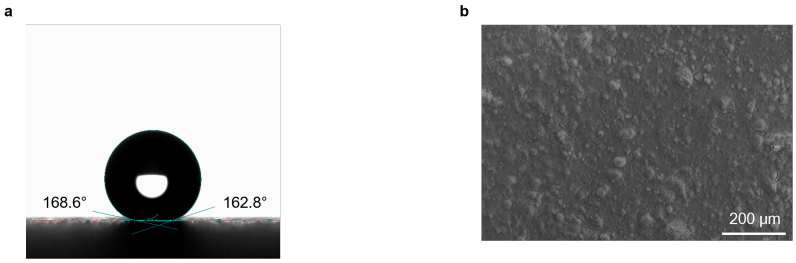


**Fig. S2** (a) Contact angles of a water droplet on a superhydrophobic coated polyethylene terephthalate sheet and (b) scanning electron microscope images of the superhydrophobic coating.

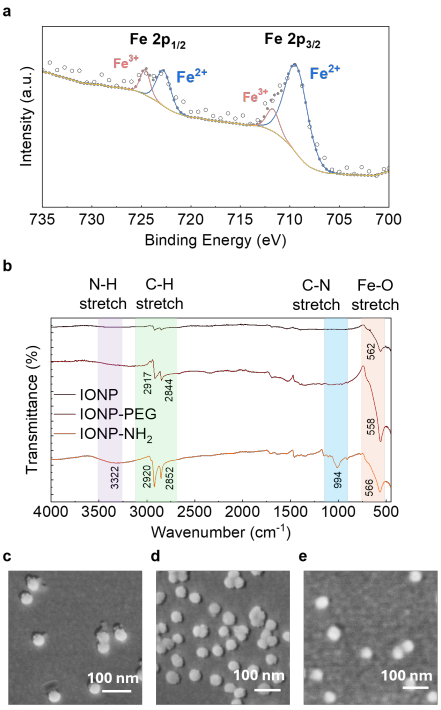


**Fig. S3** (a) XPS spectrum of the two valence states of iron in $Fe_3O_4$. The spectrum of the Fe 2p region exhibited two doublets: the peaks at 709.4 and 722.8 eV are assigned to $Fe^{2+}$, while the peaks at 711.8 and 724.6 eV are attributed to $Fe^{3+}$, corresponding to the $2p_{3/2}$ and $2p_{1/2}$ spin-orbit components, respectively. (b) FT-IR spectrum of the IONPs, demonstrating characteristic Fe-O stretching vibrations, as well as C-H stretching vibrations for alkyl chains in IONP-PEG and IONP-$NH_2$, and N-H, C-N stretching vibrations for IONP-$NH_2$. (c-e) Scanning electron microscope images of (c) IONP, (d) IONP-PEG and (e) IONP-$NH_2$.

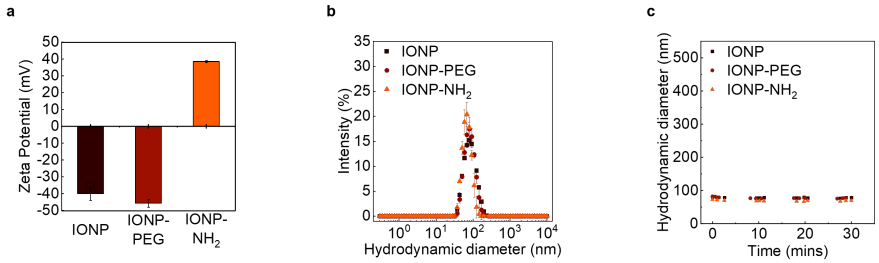


**Fig. S4** (a) Zeta potential, (b) hydrodynamic diameter distribution and (c) aggregation kinetics of IONP, IONP-PEG and IONP-$NH_2$ in water.

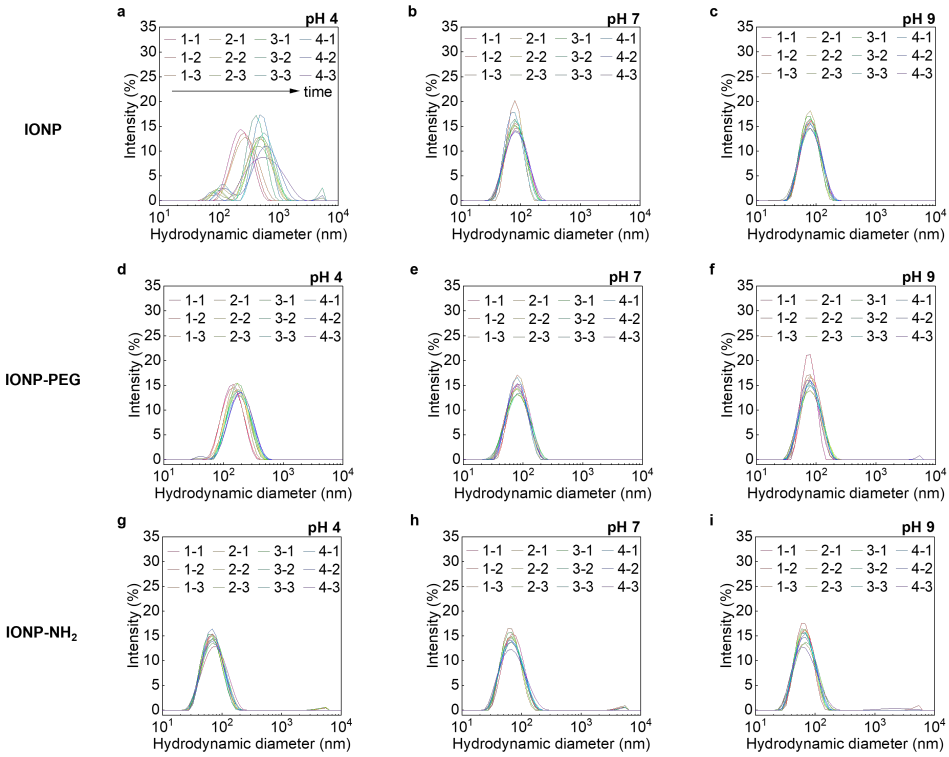


**Fig. S5** Change in hydrodynamic diameter distribution of (a-c) IONP (d-f) IONP-PEG and (g-i) IONP-$NH_2$ over time at pH 4, pH 7 and pH 9. Measurements were done in triplicates for 4 times over the course of approximately 30 minutes. The interval between triplicate measurements is approximately 5 minutes.

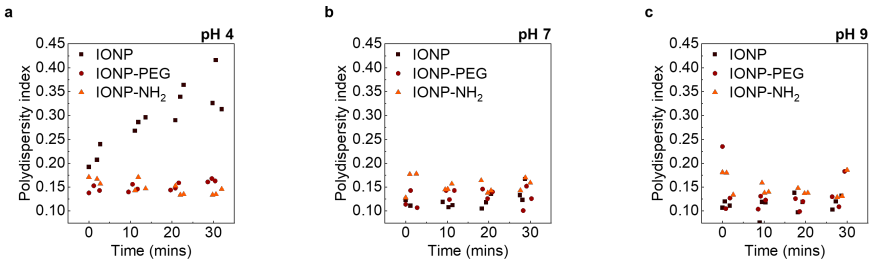


**Fig. S6** Change in polydispersity index of IONP, IONP-PEG and IONP-$NH_2$ at (a) pH 4, (b) pH 7 and (c) pH 9.

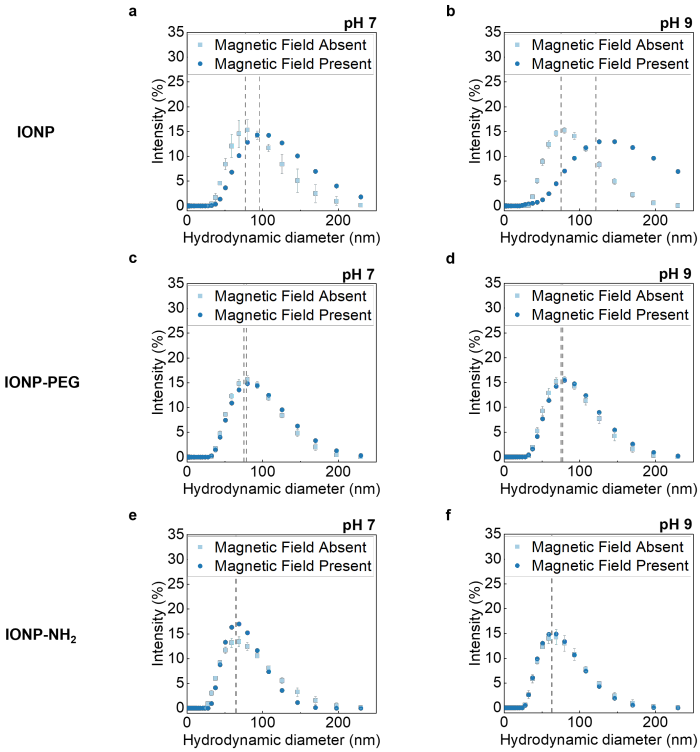


**Fig. S7** Change in hydrodynamic diameter distribution before and after application of magnetic field for (a-b) IONP, (c-d) IONP-PEG and (e-f) IONP-$NH_2$ at pH 7 and pH 9. The vertical dotted line represents the Z-average hydrodynamic diameter.

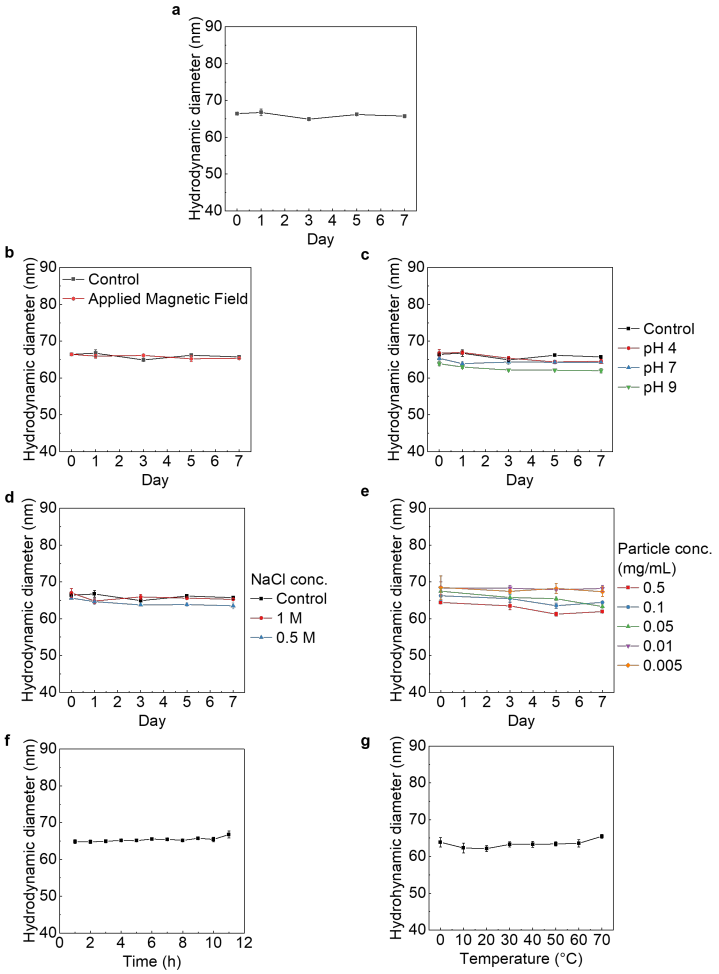


**Fig. S8** (a) Colloidal stability of IONP-$NH_2$, (b) with an applied magnetic field, (c) with varying NaCl concentrations, (d) at varying pH and (e) at varying particle concentrations over 7 days, (f) at 70 °C over 10 hours, and (g) at varying temperatures.

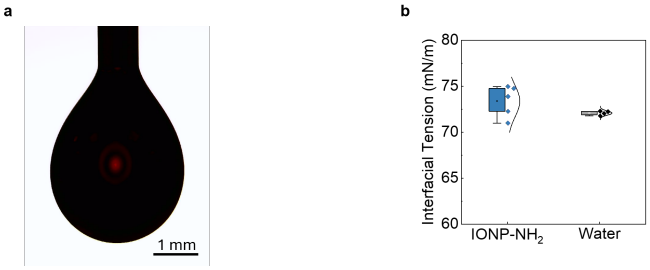


**Fig. S9** (a) Representative image and (b) surface tension of IONP-$NH_2$ compared to water, measured with the pendant drop method.

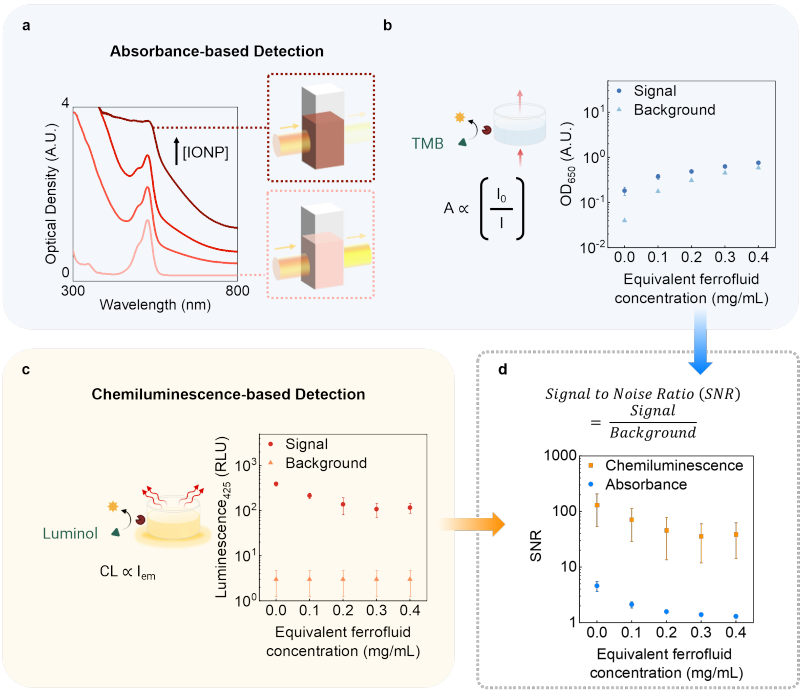


**Fig. S10** Physical compatibility of different optical detection methods with the IONP and the integrated droplet robotic device design. (a) Effect of increasing IONP concentration (0, 0.5, 1, 2 mg/mL respectively) on absorbance measurement. (b) Schematic diagram of absorbance-based detection (left) and the effect of ferrofluid on optical density signal and background (right). (Error bars: S.D., *n*=3). (c) Schematic diagram of chemiluminescence-based detection (left) and the effect of ferrofluid on chemiluminescence signal and background (right). (Error bars: S.D., *n*=3). (d) Comparison of the effect of ferrofluid on the SNR for absorbance- and chemiluminescence-based detection. (Error bars: S.D., *n*=3).

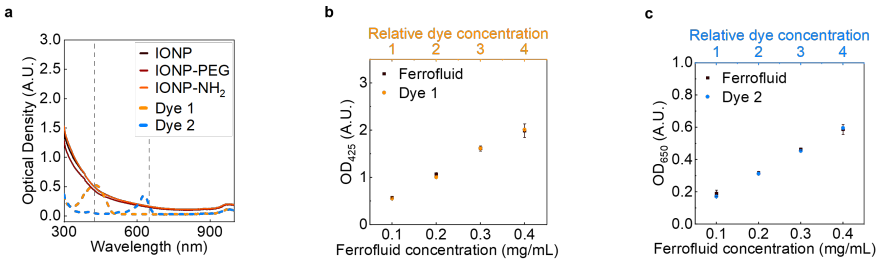


**Fig. S11** (a) Absorbance spectra of colored dyes and IONPs. (b-c) Matching colored solution concentration with the respective absorbance of ferrofluid solution concentration at (b) 425 nm for chemiluminescence measurement and (c) 650 nm for absorbance measurement.

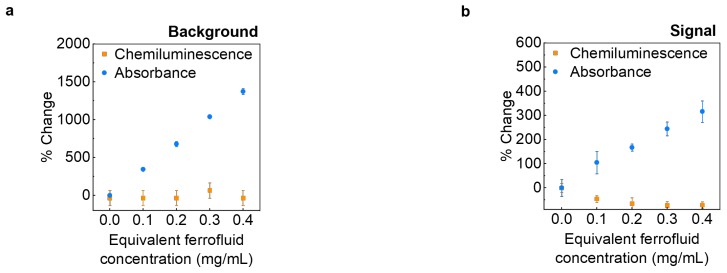


**Fig. S12** Percentage change of absorbance and luminescence signals relative to 0 mg/mL concentration for (a) background absorbance and luminescence signals and (b) absorbance and luminescence signals generated by reaction with 1.56 ng/mL HRP.

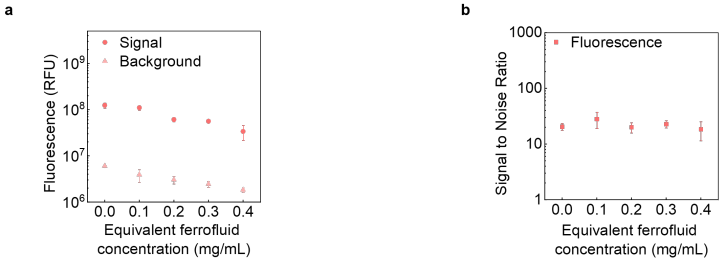


**Fig. S13** Effect of increasing ferrofluid concentration on the (a) signal and background fluorescence and (b) SNR of fluorescence-based detection.

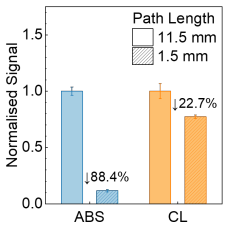


**Fig. S14** Effect of optical path length on absorbance and chemiluminescence signals.

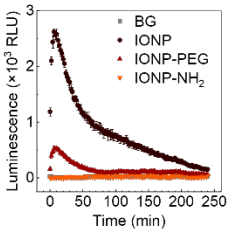


**Fig. S15** Background signals and reaction kinetics of IONP, IONP-PEG, and IONP-$NH_2$ over 4 hours.

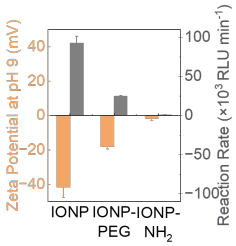


**Fig. S16** Zeta potential of the three different IONPs and their average reaction rates with luminol at pH 9 for the first 5 minutes.

| | Robust Magnetic Droplet Actuation | | | Sensitive Signal Quantification |
|---|---|---|---|---|
| | Stable at low pH | Stable at high pH | Stable with applied magnetic field | Low peroxidase activity |
| IONP | × | ✓ | × | × |
| IONP-PEG | × | ✓ | × | × |
| IONP-$NH_2$ | ✓ | ✓ | ✓ | ✓ |

**Table S1** List of functions required for conducting bioanalytical assays and the compatibility (✓) and incompatibility (×) for each IONP.

**References**


1 S. Nizamov, S. D. Sazdovska and V. M. Mirsky, *Analytica Chimica Acta*, 2022, **1204**, 339633.
2 U. Nobbmann and A. Morfesis, *Materials Today*, 2009, **12**, 52–54.
3 A. Roda and M. Guardigli, *Anal Bioanal Chem*, 2012, **402**, 69–76.
4 B. Kuswandi, Nuriman, J. Huskens and W. Verboom, *Analytica Chimica Acta*, 2007, **601**, 141–155.
5 S. Ghosh, K. Aggarwal, V. T. U., T. Nguyen, J. Han and C. H. Ahn, *Microsyst Nanoeng*, 2020, **6**, 1–18.